Correlation between the photocatalysis and growth mechanism of SnO₂ nanocrystals

IOP Publishing Journal Title
Journal **XX** (XXXX) XXXXXX https://doi.org/XXXX/XXXX

Correlation between the photocatalysis and growth mechanism of SnO_2 nanocrystals

Hongquan Zhan[1*],Ce Deng[1],Xiao-Lei Shi[2,3], Chuanqi Wu[1],Xiaohong Li[1],Zhipeng Xie[4],Changan Wang[4],and Zhi-Gang Chen[2,3*]

[1] School of Materials Science and Engineering, Jingdezhen Ceramic Institute, Jingdezhen, 333001, P.R. China.
[2] Centre for Future Materials, University of Southern Queensland, Springfield Central, Queensland 4300, Australia.
[3]School of Mechanical and Mining Engineering, The University of Queensland, Brisbane, Queensland 4072, Australia.
[4] State Key Lab of New Ceramics and Fine Processing, School of Materials Science and Engineering, Tsinghua University, 100084, Beijing, P.R. China.

E-mail: zhq_0425@163.com
E-mail:zhigang.chen@usq.edu.au; zhigang.chen@uq.edu.au

Received xxxxxx
Accepted for publication xxxxxx
Published xxxxxx

Abstract

Due to the special structural defects, SnO_2-based nanomaterials show full potentials for applying to photocatalysis. In this work, we explore the relationship between photocatalysis and growth mechanism of SnO_2 nanocrystals. Through a pH-modifying method, the growth of SnO_2 nanocrystals follows Ostwald Ripening (OR) mode at pH= 9, and Oriented Attachment (OA) mode at pH= 1.5, respectively. We comprehensively studied the structural characteristics of SnO_2 nanocrystals by investigating high-resolution transmission electron microscope, X-ray diffraction, Brunauer–Emmett–Teller nitrogen physisorption, UV-vis diffuses reflectance, and photoluminescence spectra, and the results with growth dynamic simulation show that OA mode is obviously different from OR mode, and the photocatalytic performance of SnO_2 nanocrystals varies under different growth mechanisms. The factors including crystal structure, particle size, and defects are all responsible for the variation of photocatalytic performance during OR or OA growth. Our study indicates that the photocatalytic performance of SnO_2 nanocrystals can be tuned by the controlling of crystal growth mode.

Keywords: term, term, term

1. Introduction

In-depth understanding of crystal growth mechanism provides the guidance for the structure- and property-control [1-10]. Generally, there are mainly two competitive mechanisms for the growth of nanocrystals, namely OR and OA, respectively. For OR growth, it is a classical mechanism which involves the growth of larger crystals at the expense of smaller ones [11, 12]; For OA growth, it is a novel nonclassical mechanism and can be described as that nanoparticles with common crystallographic orientations directly combine together to form larger ones [13-15]. In addition, crystal growth *via* OR or OA often shows unique characteristics. For example, OR-induced nanoparticles normally possess regular shapes and few defects, while OA-

induced nanoparticles usually have irregular morphologies and special defects, such as twins, stacking faults, and misorientations [1, 2].As a result, these morphological and structural differences may lead to different physicochemical performance. In recent years, the photoluminescence activity of CdS quantum dots related to the crystal growth mechanisms was reported by a few research groups [7, 16, 17]; However, the relationship between photocatalytical properties and growth mechanism has not been clearly revealed.

Tin dioxide (SnO_2), a typical *n*-type semiconductor with a wide band gap of ~3.6 eV, has been widely used in various areas including chemical gas sensing [8, 18], oxidation catalysis [19, 20], solar cells, and rechargeable Li batteries [21-24]. It should be noted that there exits strong links between the physicochemical properties and crystal morphology and/or structure of SnO_2 nanomaterials [25, 26], and the growth mechanism should play a significant role in determine their crystal structures, thus has attracted much attention in recent years. The earliest non-classical growth phenomenon of SnO_2 nanocrystals [27, 28] indicated that the agglomeration of SnO_2 nanoparticles in suspension induced coarsening by the OA mechanism. On this basis, hollow SnO_2 octahedra can be constructed by a template-free hydrothermal route [29]. Meanwhile, it was reported that ultrathin SnO_2 nanosheets growth follows the OA mode [30]. The studies on the OA growth [2] indicated that the crystal growth of SnO_2 nanocrystals occurred *via* the multi-step OA mechanism, and the corresponding kinetic model was established [31]. Subsequently, an aggregation-induced fast crystal growth mechanism was proposed, and the bulk-like crystals could be formed by the assembling of SnO_2 nanoparticles [32]. Furthermore, a mixed growth mode of SnO_2 nanocrystals was also discovered [33]. However, although these studies proposed the OA growth mechanism of SnO_2 nanoparticle, the relationship between the property and growth mechanism is still not clear enough, and different growth modes should result in different performances. Especially, the structure-photocatalysis relationships of SnO_2 nanocrystals directed by the OA or OR mode should be studied in detail.

In this work, under the different pH, the growth behavior of SnO_2 nanocrystals in a hydrothermal system was investigated. The growth kinetics of SnO_2 nanocrystals can be explained by the OA and OR mechanism respectively. The close link between photocatalysis, structure and growth mechanism will be discovered.

2. Experimentalsection

2.1 Synthesis

SnO_2 nanoparticles were prepared by a hydrothermal route with stannic chloride ($SnCl_4\,5H_2O$, analytical grade). To investigate the growth behavior of SnO_2 nanocrystals, the pH-modifying of the original SnO_2 nanoparticle suspension was used. One approach was the slow hydrolyzation of $SnCl_4$ solution at acidic condition: 3.15 g $SnCl_4\,5H_2O$ were dissolved in 30 mlmixed solution of 15 mldeionized water and 15 ml ethanol, and another was the forcible hydrolyzation of $SnCl_4$ solution at alkali condition: 3.15 g $SnCl_4\,5H_2O$ were dissolved in 25 ml mixed solution of 10 ml deionized water and 15 ml ethanol, and subsequently added 5 ml ammonia water to keep the pH value at~9. The suspension was uniformly stirred and finally transferred into a 60 ml Teflon-lined autoclave for consequence hydrothermal reaction. The hydrothermal reaction was conducted at 220 ^{o}C in an oven for different durations, ranging from 2 hours to 7 days. When the reaction was completed, the autoclave was removed from the oven and cooled down to room temperature. The samples were centrifugally separated and sufficiently washed by deionized water and ethanol to remove the residual impurities. Finally, the products were placed into a desiccator for drying at 60 ^{o}C for 24 hours.

2.2Characterization

The crystal structures were identified by X-ray diffraction (XRD) on a Rigaku D/MAX 2200 VPC diffractometer, operating at 40 kV and 20 mA, with steps of 0.02^{o} at 10^{o} min^{-1} in a 2θ range from 15^{o} to 75^{o}. The crystal morphological and structural characteristics were further examined by transmission electron microscopy (TEM, JEM-2010HR electron microscope equipped with a Gatan GIF system) with an acceleration voltage of 200 kV. The Brunauer–Emmett–Teller (BET) nitrogen physisorption experiments were carried out on a Micromeritics ASAP 2010 system. The pore size distributions of synthesized products were determined by using the Barrett-Joyner-Halenda (BJH) algorithm according to the desorption data of the N_2 isotherms. Photoluminescence (PL) spectra of the samples were obtained using a Renishaw micro-Raman model *via* Reflex spectrograph with the excitation wavelength of 325 nm and the spectrum range was extended to 380–800 nm. UV-vis diffuses reflectance spectra of the samples were recorded on Lamda850 spectrophotometer in the range of 200-800 nm.

2.3Photocatalytic activity evaluation

The photocatalytic activity for the degradation of methyl orange (MO) was performed in a Pyrex reactor, in which 200 mg of the photocatalysts was suspended in 200 mlof MO aqueous solution (10 mg Ł$^{-1}$). A 250 W mercury lamp (Beijing Perfect Co., Ltd., the wavelength within the range of 365 nm) as an ultraviolet light source was positioned inside a cylindrical Pyrex vessel. Prior to irradiation, the suspension of the photocatalyst in MO aqueous solution was stirred in

the dark for 30 min to secure an adsorption/desorption equilibrium. At the given irradiation time intervals of 20 min, 4 mlaliquots were sampled and separated by centrifugation, and the residual MO concentration in the supernatants was analyzed by UV-vis spectroscopic measurements (T6 spectrophotometer, Beijing Purkinje General Instrument Co., Ltd.). The concentration of MO was determined by monitoring the change in the absorbance at 464 nm.

3. Results and discussion

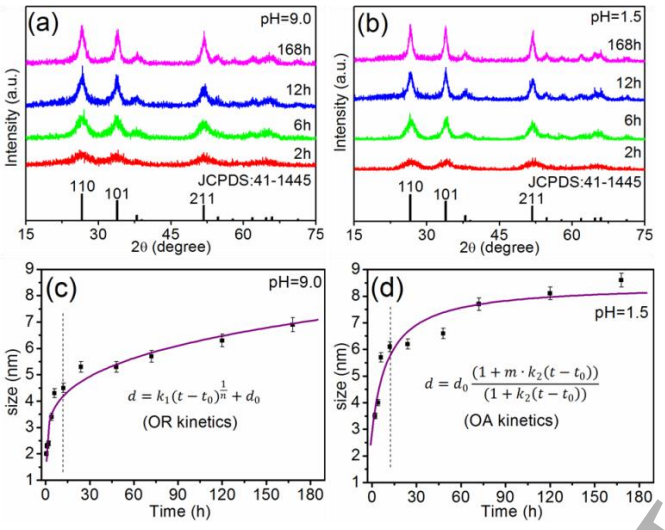

Figure 1. XRD patterns of SnO_2 specimens synthesized at 220 °C with different reaction times ranging from 2 to 168 hours under (a) pH=~9.0 and (b) pH= ~1.5, (c) When pH= ~9.0, SnO_2 nanoparticle size (square dots with error bar) fit well witha typical OR kinetic model (purple lines), and(d) when pH= ~1.5, SnO_2 nanoparticle size (square dots with error bar) fit well with a typical OA kinetic model (purple lines).

Table 1 Simulated data for the crystal growth of SnO_2 nanoparticles under different pH

	R^2	d_0	n/m	k
pH= ~9.0	0.93	1.72	n=3.57	k_1=1.24
pH= ~1.5	0.88	3.17	m=2.66	k_2=0.08

SnO_2 nanocrystals were synthesized under different conditions. One was the forcible hydrolyzation of $SnCl_4$ solution with using aqueous ammonia under hydrothermal condition; while another was the slow hydrolyzation of $SnCl_4$ solution without using aqueous ammonia under the same condition. In this situation, SnO_2 nanocrystals should grow in different pH, where the former is ~9.0 and the latter is ~1.5 according to the pH testing. At pH= ~1.5, the acidic condition is derived from the hydrochloric acid produced from the hydrolysis of $SnCl_4$. Figures **1**(a) and **1**(b) show XRD patterns of the hydrothermal products synthesized from different reaction durations under two conditions, from which all diffraction peaks can be indexed as tetragonal rutile structure of SnO_2 (JCPDS NO. 41–1445). With increasing the hydrothermal reaction duration,the diffraction peaks of products are visibly enhanced. The weak diffraction peak appeared after a reaction of 2 hours, indicating the initiation of crystalline phase. With the prolongation of reaction duration, the intensities and sharpness of diffraction peaks increase, indicating a continuous increase of crystallinity and crystal size.

The average crystal size of samples can be calculated by Scherrer equation from the full width at half-maximum (FWHM) of (110) diffraction peaks [34]:

$$d=0.89\lambda/(\beta\cos\theta) \quad (1)$$

where d is the crystal particle size, λ is the X-ray wavelength (λ= 0.1541 nm), β is FWHMof (110) diffraction peak, and θ is the Bragg diffraction angle, respectively. Figures **1**(c) and **1**(d) plot the calculated crystallite sizes as a function of reaction timeunder different pH, respectively. It is clearly seen that the particle size at pH= ~1.5 is much larger than that at pH= ~9.0. Meanwhile, atthe initial stage (before about 12 hours), the growth rate of SnO_2 nanocrystals at pH= ~1.5 increases with a faster process. The results of the crystallite sizes indicate that the growth of SnO_2 should have different crystallization behaviors at different pH conditions, which can be further confirmed by electron microscopy.

It has been reported that the surface charge of nanoparticles plays a critical role in the interactions between nanoparticles [35]. Previous study indicated that the isoelectric point of SnO_2 nanoparticles was~3.1 [28]. In this situation, the surface charge is almost neutral and the aggregation behavior of SnO_2 nanoparticles should be enhanced at pH= ~1.5 (near the isoelectric point). With increasing the solution pH (up to pH= ~9.0), the repulsive forces between nanoparticles and the negatively charged anions increase, leading to a decrease in the nanoparticle size. Clearly, the growth mode of SnO_2 at pH= ~9.0 should follow the OR mechanism; while the growth mode at pH= ~1.5 should be determined by the OA mechanism. To confirm this speculation, the simulation has been conducted according to the OR model and OA model, respectively. The growth kinetics of SnO_2 at pH= ~9.0 can be described and fitted by the OR model [36, 37]:

$$d=k_1(t\text{-}t_0)^{1/n}+d_0 \quad (2)$$

where t is the time, t_0 is the induction time (here t_0= 0.5 hours), d is the average crystallite size at t, d_0 is the initial average crystallite size at the starting point, k_1 is a temperature-dependent reaction rate constant, and n is an exponent, respectively. Figure **1**(c) and Table **1** show that the fitted data well matched with the experimental results. The fitting parameter n was 3.57, suggesting that the crystal

growth was mainly controlled by the dissolution and precipitation process based on the OR mechanism (when n=4, the growth is controlled by dissolution kinetics at the particle-matrix interface) [38].

For the growth at pH= ~1.5, the OA model can be used to simulate the growth process of SnO_2 nanocrystals [36, 37]:

$$d=d_0((1+mk_2(t-t_0))/((1+k_2(t-t_0)) \quad (3)$$

where t is the time, t_0 is the induction time (here t_0= 0.5 hours), d is the average crystallite size at t, d_0 is the initial average crystallite size at the starting point, m is defined as the aggregation factor which represents the degree of crystal combination, and k_2 represents the crystal growth rate constant, respectively. The fitting curve shown in Figure **1**(d) well align with the experiment results, indicating the actual crystal growth based on theOA mechanism. The deduced parameter m was 2.66, revealing that the growth was along the OA mode of multiple nanoparticles rather than the typical OA mode.

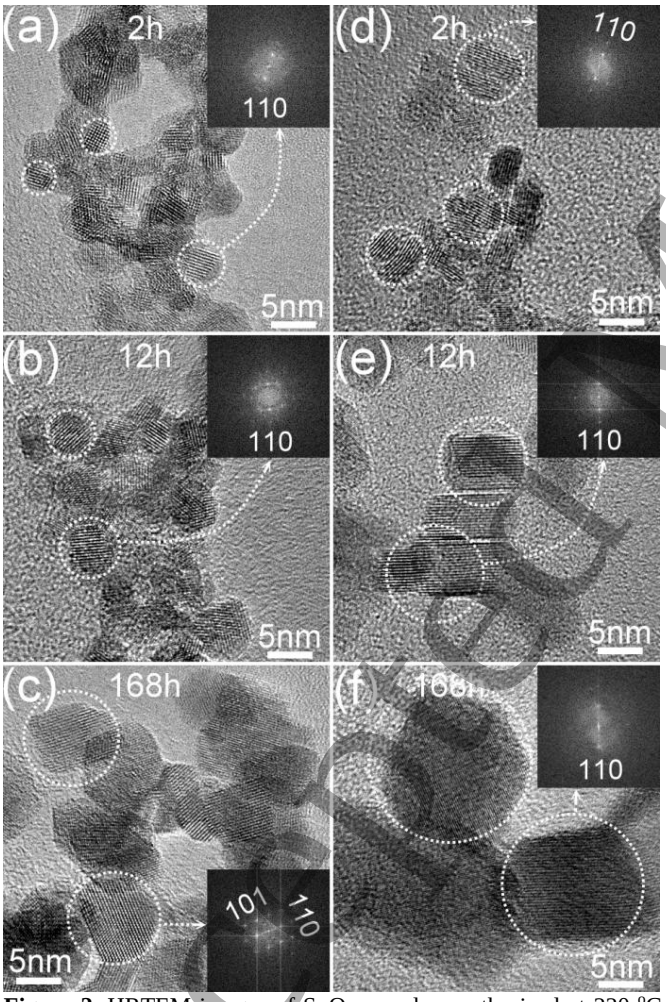

Figure 2. HRTEM images of SnO_2 samples synthesized at 220 ^oC with reaction time for (a, d) 2 hours, (b, e) 12 hours, and (c, f) 168 hours under different pH, where the left column is at pH= ~9.0, and the right column is at pH= ~1.5. The inserts are corresponding FFT patterns from the HRTEM areas marked by the dashed circle lines.

Based on the analysis above, we can conclude that with different pH, SnO_2 nanocrystals grow along different pathways. To understand the structural evolution of SnO_2 under two conditions, high-resolution TEM (HRTEM) were performed. Figure **2** shows typical HRTEM images of the products synthesized from different reaction time, the insets show their corresponding Fast Fourier transform (FFT) patterns. The left column is at pH= ~9.0, and the right column is at pH= ~1.5. As can be seen, under different conditions, with the prolongation of hydrothermal reaction time, the crystallinity and crystal size of SnO_2 nanoparticles increase, which is consistent with the XRD results. On the left column, the particles formed by means of the OR mode show a continuous increase of size and maintain a roughly spherical shape. Figure **2**(a) is the HRTEM image of the sample synthesized for 2 hours, and the inset shows corresponding FFT patterns. It is obvious that the average crystal size is ~2.5 nm, and the crystallization is weak based on its FFT pattern. The unclear lattice fringe and rough surface of the crystals indicate the presence of the defects. With the reaction proceeding to 12 hours, the crystal size became larger, and the samples kept a sphere morphology. When the reaction time was up to 168 hours, the crystals significantly grew up to ~7 nm, and the crystal surfaces became much smoother. Clearly, as shown in Figure **2**(c), the clear lattice fringe and strong diffraction spots both indicate that the crystals are perfect and most of the defects should disappear. This growth process matches well with the behavior of the OR mode.

On the right column, the particles show different growth pattern. Figure **2**(d) is a HRTEM image of the sample synthesized for 2 hours, from which the particle is composed of several sub-nanocrystals agglomerating along specific crystallographic orientation. Due to the OA mode of sub-nanocrystals, the particles show an elongated shape and sizes are up to 3.5 nm, which is noticeably larger than that of the OR mode. The discontinuous lattice fringes, rough surfaces, and irregular morphology also indicate the presence of defects. Especially, the interfaces between the sub-nanocrystals can be directly observed by HRTEM, where intensive interface defects can be discovered, derived from the noncompact combination of sub-nanocrystals. With increasing the reaction duration to 12 hours (Figure **2**(e)), the particle size significantly increased. Due to the mutual fusion of sub-nanocrystals, the particle surfaces become much more regular and smoother; however, it is still clear to observe interface defects in the crystals. When the reaction time reaches to 168 hours (Figure **2**(f)), the maximum size of ~9 nm can be achieved, which results from the rapid aggregation growth. The regular crystal shape and clear lattice fringe confirm the achievement of perfect crystals, and there is no obvious defect found. It is interesting that the corresponding

FFT pattern shows a single-crystal feature, even though the particles aggregated from smaller crystals at the beginning. Under the OA mechanism, the crystal growth process was obviously different from the OR growth. The special morphology, larger size, and interface defects indicate different characteristic. More evidences by TEM can be seenin the Supporting Information.

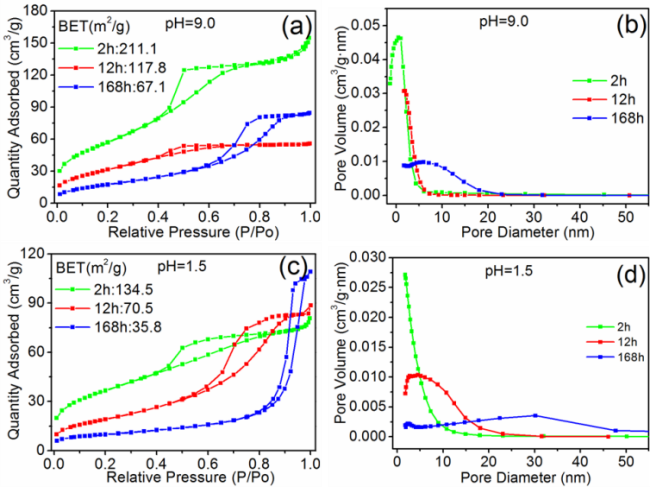

Figure 3. Nitrogen adsorption/desorption isotherms and BJH pore size distribution plots of SnO_2 samples synthesized at 220 ^oC for different reaction durations under different pH. Here (a, b) pH= ~9.0 and (c, d) pH= ~1.5.

Figure **3** shows the nitrogen adsorption/desorption isotherms and pore size distribution of SnO_2 samples synthesized at 220 ^oC, the specific surface area and pore-size distribution are determined by BET equation and BJH method. The adsorption/desorption isotherm curves reflect a typical IV adsorption model, and the adsorption capacity improves with increasing the relative pressure. Meanwhile, with increasing the reaction duration, the BET surface area of samples produced by the OR and OA modes shows a decreasing trend; however, it is obvious that the samples produced by the OR mode have more significant surface area than that of the samples grown by the OA mode. Because of growing with the OA mode, the aggregated growth between nanoparticles should lead to a significant decreasing of the surface area. Although the surface area decreases, the microporous structure can be formed at the initial stage. As shown inFigure **3**(d), the samples synthesized for 2 hours exhibited the narrow micropore size distribution centered at 1.8 nm, which can also be seen from HRTEM shown in Figure **2**(d). The pseudo pore structure can be found in Figure **3**(b), which is attributed to the agglomeration of the smaller nanocrystals to reduce the surface energy. It is not real microporous structure, which can be further verified from HRTEM image shown in Figure **2**(a).

To study the defects of the samples, the PL spectra are investigated, and the results are shown in Figure **4**. Under these two OR/OA modes, the evolution trend of PL spectra is notably different. During the OR growth, as shown in Figure **4**(a), the broad peak around 500 nm (green luminescence) is observed, which is attributed to the internal defects such as dislocations, vacancies, and dangling bonds [7, 39]. Apparently, the defect-induced PL at 2 hours shows the highest peak, which is derived from a large number of internal defects produced during the nucleation process. With the times proceeding, these internal defects reduce, and the peak is weaken to the lowest at 6 hours. From 6 to 12 hours, the PL intensity is slightly enhanced. According to the reference, the imperfections degree and the crystallinity of the nanocrystals play important rolesin the PL [40]. During this stage, with the imperfection structure (Figure **2**(b)), the size increases and the degree of crystallization improves. All these factors contribute to enhance the luminescence modestly. After 12 hours, the luminescence intensity gradually decreases due to that the nanocrystals grow perfectly and the internal defects almost disappear.

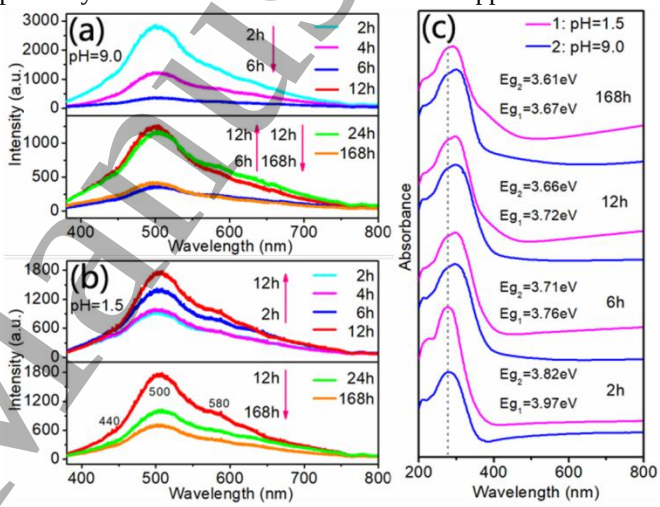

Figure 4. (a, b) Evolution characteristics of the PL spectra of SnO_2 nanoparticles synthesized at 220 ^oC under different pH. Here (a) pH= ~9.0, and (b) pH= ~1.5. (c) UV-vis diffuse reflectance spectra of SnO_2 samples synthesized at 220 ^oC for different reaction durations under different pH, where blue line represents pH= ~9.0, and pink line represents pH= ~1.5.

During the OA growth, as shown in Figure **4**(b), the broad peak around 500 nm is also observed including the shoulder peaks at ~580 nm and 440 nm. The shoulder peak at~580 nm (yellow luminescence) is attributed to the defects from the oxygen vacancies formed in SnO_2 surface [41, 42]. The other shoulder peak at 440 nm (blue luminescence) results from the structural defects. In addition, many burr peaks can be seen from 400 nm to 600 nm, which should result from the interface defects from the Oriented Attachment between the nanoparticles [7]. According to the PL results shown in Figure **4**(b), the entire process can be divided into two stages. At the first stage from 2 to 12 hours, with increasing the synthesis duration, PL intensity significantly increase. Using the OA growth, the combination of several primary particles

can result in a high concentration of the OA-induced defects such as dislocations, misorientations, and interface defects between these initial particles. During this period, more nanoparticles agglomerated and the concentration of the OA-induced defects increased, resulting in an improving of PL. At the second stage (after 12 hours), the PL intensity slowly decreased, which was derived from the self-integration of the nanostructures. Therefore, it can be concluded that the PL behaviors are directly related to the crystal growth process.

To study the optical response of the samples from different growth mechanisms, the UV−vis diffuse reflectance spectra were explored, as shown in Figure **4**(c). The shape and absorption peak of the diffuse reflectance are slightly different in the process of crystal growth. To compare the spectra of two growth modes, the trends are comparatively unanimous. The absorption band at 280 nm reveals that SnO_2 nanocrystals have strong absorption ability in the ultraviolet region. With continuing the reaction, the absorption peak remarkably showed a red-shift and broadening effect, which is beneficial to the light absorption. This is attributed to the increasing of particle size and the enhancing of crystallization. The value of bang gap (E_g) can be calculated by Wood and Tauc method [43]. The E_g data indicates that the band gap become narrow with the reaction going on.

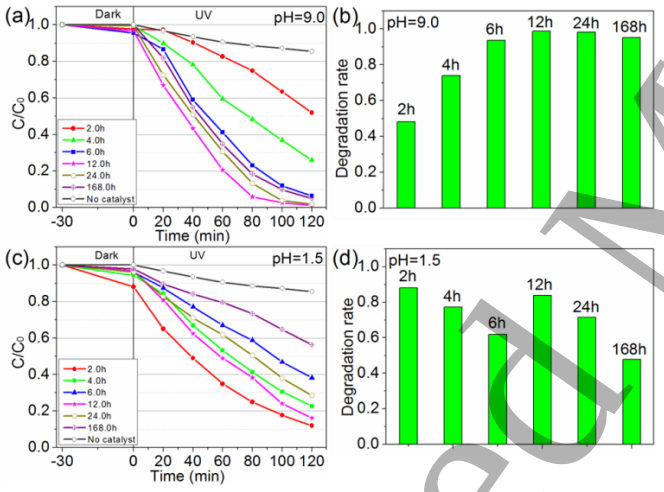

Figure 5. (a, c) Comparison of photocatalytic activities of SnO_2 samples synthesized at 220 °C under different pH. (b, d) The degradation rate of MO in the presence of SnO_2 nanocrystals synthesized for different reaction durations, where (a, b) pH= ~9.0, and (c, d) pH= ~1.5.

The photocatalytic degradation of MO in aqueous solution under ultraviolet light is further depicted in Figure **5**. As can be seen, SnO_2 nanoparticles produced from different growth mechanisms present different behaviors in the photocatalytic activity. At pH= ~9.0, with prolonging the crystallization time, the degradation ability to MO increases and reaches a maximum value within 12 hours. After that, the photocatalytic activity of the samples remains almost stable, although a slight decrease can be seen with increasing the time. For pH= ~1.5, at the initial stage (from 2 to 6 hours), the photocatalytic activity of the samples shows an opposite trend, which decreases rapidly with the crystallization time increasing. Atthe second stage (from 6 to 12 hours), the photocatalytic activity increases again. At the last stage (After 12 hours), the degradation of MO tends to be decreased gradually.

Distinctly, the different growth modes resulted in different photocatalytic activity. In general, the photocatalytic properties are closely related to crystallization degree, crystal microstructure, particle size, surface area, and defects [10, 44-46]. All these factors play important roles in the absorption of light and adsorption of organic pollutants, which are two key factors to the photocatalytic activity. During OR growth, with the extension of time, the crystal crystallinity is enhanced, and the band gap is narrowed. As a result, the absorption of light is increased, and the photocatalytic performance is gradually improved at the initial stage. After 12 hours, due to the larger particle size and the smaller specific surface area, the adsorption of the samples is weakened, which counteracts the influence of band gap narrowing, and the photocatalytic performance keeps stable.

However, during the OA growth, the sample synthesized at 2 hours shows the best catalytic performance. Owing to the Oriented Attachment between the nanoparticles, there is special microporous structure and many OA-induced defects formed in SnO_2 nanocrystals (as described in Figures **2** and **3**). With the larger surface area and the special microporous structure, this sample has excellent absorption ability, which can be further verified by the adsorption data of dark field in Figure **5**(c). In addition, the special microporous structure can improve the charge separation and migration of photogenerated carriers through interparticle charge transfer [47, 48]. Moreover, the OA-induced defects also play a significant role in facilitate the separation of the e^-/h^+ pairs because the photogenerated holes may easily find their way through the defects to travel to the interface and react with the organic pollutants. Therefore, all these factors are beneficial to improving the photocatalytic activity.

Finally, based on the above analysis, the photocatalytic activity of SnO_2 nanocrystals is discovered to directly relate to the growth process. As shown in Figure **6**, under the different growth modes, the photocatalytic degradation rate dependence on the structural evolution is illustrated in one scheme. Visibly, in the initial stage (from 2 to 6 hours), the photocatalytic activity of SnO_2 prepared by different methods shows an opposite tendency respectively, which is upward trend under the OR mode and downward under the OA mode. Due to the special microporous structure and OA-induced defects, the OA-samples of 2 hours reveal better photocatalytic property. After 12 hours, under the OR mode, the photocatalytic activity reaches the highest level and

subsequently keeps stable. While, under the OA mode, a gradual decrease trend appears with growth process because of self-integration of the nanocrystals.

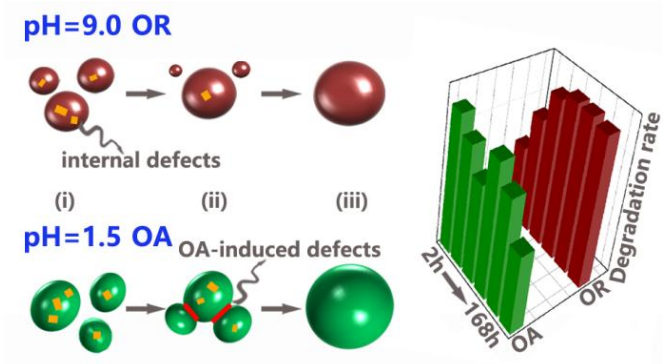

Figure 6. Schematic drawing to show the correlation between the growth evolution and photocatalysis of SnO_2 nanocrystals under different pH.

4. Conclusion

SnO_2 nanocrystals were synthesized along different ways, one approach consisted of a hydrothermal technique at alkali condition, and another comprised a hydrothermal treatment at acidic condition. Through the crystal growth dynamics, the growth pattern of SnO_2 at pH= ~9.0 follows the classic OR mode while the growth pattern at pH= ~1.5 can be described by the OA mode. Under the OA mechanism, the crystal growth process is obviously different from the OR growth. The special microporous structure, larger size, and OA-induced defects display different characteristic. The photocatalytic degradation rate of MO is revealed to directly relate to the growth process of SnO_2 nanocrystals, which shows the different behavior according to different growth mechanism. The correlation between photocatalytic performance and crystal growth mechanism are revealed, and the synthesizing route of nanocrystals with excellent photocatalytic performance is also proposed.

Acknowledgements

This work was financially supported by National Natural Science Foundation of China (No: 21661017), Natural Science Foundation of Jiangxi Province (No: 20161BAB203081), Foundation of Jiangxi Provincial Department of Education (No: GJJ170795, GJJ180718) and Australian Research Council.

References

[1] Dalmaschio C J, Ribeiro C and Leite E R 2010 Impact of the colloidal state on the oriented attachment growth mechanism *Nanoscale* **2** 2336-45

[2] Zhang J, Huang F and Lin Z 2010 Progress of nanocrystalline growth kinetics based on oriented attachment *Nanoscale* **2** 18-34

[3] Jehannin M, Rao A and Cölfen H 2019 New Horizons of Nonclassical Crystallization *J. Am. Chem. Soc*. **141** 10120-36

[4] Zhang Q, Mayoral A, Terasaki O, Zhang Q, Ma B, Zhao C, Yang G J and Yu J H 2019 Amino Acid-Assisted Construction of Single-Crystalline Hierarchical Nanozeolites *via* Oriented-Aggregation and Intraparticle Ripening *J. Am. Chem. Soc*.**141** 3772-6

[5] Yu B B, Zhang X, Jiang Y, Liu J, Gu L, Hu J S and Wan L J 2015 Solvent-Induced Oriented Attachment Growth of Air-Stable Phase-Pure Pyrite FeS_2 Nanocrystals *J. Am. Chem. Soc*. **137** 2211-4

[6] Huang Y, Lin J, Li L, Xu L L, Wang W J, Zhang J, Xu X W, Zou J and Tang C C 2015 High performance UV light photodetectors based on Sn-nanodot-embedded SnO_2 nanobelts *J. Mater. Chem. C* **3** 5253-8

[7] Zheng J S, Huang F, Yin S G, Wang Y J, Lin Z, Wu X L and Zhao Y B 2010 Correlation between the Photoluminescence and Oriented Attachment Growth Mechanism of CdS Quantum Dots *J. Am. Chem. Soc*. **132** 9528-30

[8] Xu X X, Zhuang J and Wang X 2008 SnO_2 Quantum Dots and Quantum Wires: Controllable Synthesis, Self-Assembled 2D Architectures, and Gas-Sensing Properties *J. Am. Chem. Soc*.**130** 12527-35

[9] Hughes B K, Blackburn J L, Kroupa D, Shabaev A, Erwin S C, Efros A L, Nozik A J, Luther J M and Beard M C 2014 Synthesis and spectroscopy of PbSe fused quantum-dot dimers *J. Am. Chem. Soc*. **136** 4670-9

[10] Zhan H Q, Chen Z G, Zhuang J L, Yang X F, Wu Q L, Jiang X P, Liang C L, Wu M M and Zou J 2015 Correlation between Multiple Growth Stages and Photocatalysis of $SrTiO_3$ Nanocrystals *J. Phys. Chem. C* **119**3530-7

[11] Speight M V 1968 Growth kinetics of grain-boundary precipitates *Acta Metall*. **16** 133-5

[12] Kirchner H O K 1971 Coarsening of grain-boundary precipitates *Metall. Trans*. **2** 2861-4

[13] Penn R L and Banfield J F 1998 Imperfect oriented attachment: dislocation generation in defect-free nanocrystals *Science* **281** 969-71

[14] Li D S, Nielsen M H, Lee J R, Frandsen C, Banfield J F and De Yoreo J J 2012 Direction-specific interactions control crystal growth by oriented attachment *Science* **336** 1014-18

[15] Lee E J H, Ribeiro C, Longo E and Leite E R 2005 Oriented Attachment: An Effective Mechanism in the Formation of Anisotropic Nanocrystals *J. Phys. Chem. B* **109** 20842-6

[16] Jeong D W and Jang D J 2018 Rapid Stepwise Growth of Water-Dispersive CdS Quantum Dots in Ethylene Glycol *Cryst. Growth Des*. **18** 4945-51

[17] Xue X G, Zhuang Z Y, Huang F and Lin Z 2013 Understanding the Occurrence of the Maximum Band-Edge Photoluminescence of TGA-Capped CdS QDs *via* Growth Kinetic Study *Cryst. Growth Des*. **13** 5220-8

[18] Han X G, Jin M S, Xie S F, Kuang Q, Jiang Z Y, Jiang Y Q, Xie Z X and Zheng L 2009 Synthesis of tin dioxide octahedral nanoparticles with exposed high-energy {221} facets and enhanced gas-sensing properties *Angew. Chem., Int. Ed*. **48** 9180-3

[19] Sun Y F, Lei F C, Gao S, Pan B C, Zhou J F and Xie Y 2013 Atomically thin tin dioxide sheets for efficient catalytic

oxidation of carbon monoxide *Angew. Chem., Int. Ed*. **52** 10569-72

[20] Zhang W Y, Qin Q, Dai L,Qin R X, Zhao X J, Chen X M, Ou D H, Chen J, Chuong T T, Wu B H and ZhengN F 2018 Electrochemical Reduction of Carbon Dioxide to Methanol on Hierarchical Pd/SnO_2 Nanosheets with Abundant Pd–O–Sn Interfaces *Angew. Chem., Int. Ed*. **57** 9475-9

[21] Wang C, Zhou Y, Ge M Y, Xu X B, Zhang Z L and Jiang J Z 2010 Large-Scale Synthesis of SnO_2 Nanosheets with High Lithium Storage Capacity *J. Am. Chem. Soc*. **132** 46-7

[22] Chen J S and Lou X W 2012 SnO_2 and TiO_2 nanosheets for lithium-ion batteries *Mater.Today* **15** 246-54

[23] Wang L P Y, Leconte Y, Feng Z X, Wei C, Zhao Y, Ma Q, Xu W Q, Bourrioux S, Azais P, Srinivasan M and Xu Z C J 2017 Novel Preparation of N-Doped SnO_2 Nanoparticles *via* Laser-Assisted Pyrolysis: Demonstration of Exceptional Lithium Storage Properties *Adv. Mater*. **29** 1603286-97

[24] Dong W J, Xu J J, Wang C, Lu Y, Liu X Y, Wang X, Yuan X T, Wang Z, Lin T Q, Sui M L, Chen I W and Huang F 2017 A Robust and Conductive Black Tin Oxide Nanostructure Makes Efficient Lithium-Ion Batteries Possible *Adv. Mater*. **29** 1700136-44

[25] Das S and Jayaraman V 2014 SnO_2: A comprehensive review on structures and gas sensors*Prog. Mater. Sci*. **66** 112-255

[26] Chen Z W, Pan D Y, Li Z, Jiao Z, Wu M H, Shek C H, Wu C M L and Lai J K L 2014 Recent advances in tin dioxide materials: some developments in thin films, nanowires, and nanorods *Chem. Rev*. **114** 7442-86

[27] Leite E R, Giraldi T R, Pontes F M, Longo E, Beltrán A and Andrés J 2003 Crystal growth in colloidal tin oxide nanocrystals induced by coalescence at room temperature *Appl. Phys. Lett*. **83** 1566-8

[28] Ribeiro C, Lee E J H, Giraldi T R, Longo E, Varela J A and Leite E R 2004 Study of Synthesis Variables in the Nanocrystal Growth Behavior of Tin Oxide Processed by Controlled Hydrolysis *J. Phys. Chem. B* **108** 15612-7

[29] Yang H G and Zeng H C 2004 Self-construction of hollow SnO_2 octahedra based on two-dimensional aggregation of nanocrystallites *Angew. Chem., Int. Ed*. **43** 5930-3

[30] Wang C, Du G H, Ståhl K, Huang H X, Zhong Y J and Jiang J Z 2012 Ultrathin SnO_2 Nanosheets: Oriented Attachment Mechanism, Nonstoichiometric Defects, and Enhanced Lithium-Ion Battery Performances *J. Phys. Chem. C* **116** 4000-11

[31] Zhuang Z Y, Zhang J, Huang F, Wang Y H and Lin Z 2009 Pure multistep oriented attachment growth kinetics of surfactant-free SnO_2 nanocrystals *Phys. Chem. Chem. Phys*. **11** 8516-21

[32] Zhuang Z Y, Huang F, Lin Z and Zhang H Z 2012 Aggregation-induced fast crystal growth of SnO_2 nanocrystals *J. Am. Chem. Soc*.**134** 16228-34

[33] Zhang Y L, Li L P, Zheng J, Li Q, Zuo Y, Yang E R and Li G S 2015 Two-Step Grain-Growth Kinetics of Sub-7 nm SnO_2 Nanocrystal under Hydrothermal Condition *J. Phys. Chem. C* **119** 19505-12

[34] Patterson A L 1939 The Scherrer Formula for X-Ray Particle Size Determination *Phys. Rev*. **56** 978-82

[35] Mudunkotuwa I A and Grassian V H 2010 Citric Acid Adsorption on TiO_2 Nanoparticles in Aqueous Suspensions at Acidic and Circumneutral pH: Surface Coverage, Surface Speciation, and Its Impact on Nanoparticle−Nanoparticle Interactions *J. Am. Chem. Soc*. **132** 14986-94

[36] Zhan H Q, Yang X F, Wang C M, Liang C L and Wu M M 2010 Multiple Growth Stages and Their Kinetic Models of Anatase Nanoparticles under Hydrothermal Conditions *J. Phys. Chem. C* **114** 14461-6

[37] Zhan H Q, Yang X F, Wang C M, Chen J, Wen Y P, Liang C L, Greer H F, Wu M M and Zhou W Z 2012 Multiple Nucleation and Crystal Growth of Barium Titanate *Cryst. Growth Des*. **12** 1247-53

[38] Huang F, Zhang H Z and Banfield J F 2003 Two-Stage Crystal-Growth Kinetics Observed during Hydrothermal Coarsening of Nanocrystalline ZnS *Nano Lett*. **3** 373-8

[39] Zhang G Z, Xie C S, Zhang S P, Zhang S S and Xiong Y 2014 Defect Chemistry of the Metal Cation Defects in the p- and n-Doped SnO_2 Nanocrystalline Films *J. Phys. Chem. C* **118** 18097-109

[40] Zhan H Q, Jiang X P, Zhu M X, Li X H, Luo Z Y and Shu K Z 2016 Photoluminescence activity of $BaTiO_3$ nanocrystals dependence on the structural evolution *J. Cryst. Growth* **433** 80-5

[41] Kar A, Kundu S and Patra A 2011 Surface Defect-Related Luminescence Properties of SnO_2 Nanorods and Nanoparticles *J. Phys. Chem. C* **115** 118-24

[42] Sun S H, Meng G W, Zhang G X, Masse J P and Zhang L D 2007 Controlled growth of SnO_2 hierarchical nanostructures by a multistep thermal vapor deposition process *Chem. Eur. J*. **13** 9087-92

[43] Souza A E, Santos G T A, Barra B C, Macedo W D, Teixeira S R, Santos C M, Senos A M O R, Amaral L and Longo E 2012 Photoluminescence of $SrTiO_3$: Influence of Particle Size and Morphology *Cryst. Growth Des*. **12** 5671-9

[44] Chen X B, Shen S H, Guo L J and Mao S S 2010 Semiconductor-based Photocatalytic Hydrogen Generation *Chem. Rev*. **110** 6503-70

[45] Zhan Z B, Xu R, Mi Y, Zhao H P and Lei Y 2015 Highly Controllable Surface Plasmon Resonance Property by Heights of Ordered Nanoparticle Arrays Fabricated via a Nonlithographic Route *ACS Nano* **9** 4583-90

[46] Zhan Z B, Grote F, Wang Z J, Xu R and Lei Y 2015 Degenerating Plasmonic Modes to Enhance the Performance of Surface Plasmon Resonance for Application in Solar Energy Conversion *Adv. Energy Mater.* **5** 1501654

[47] Zhou W, Li W, Wang J Q, Qu Y, Yang Y, Xie Y, Zhang K F, Wang L, Fu H G and Zhao D Y 2014 Ordered Mesoporous Black TiO_2 as Highly Efficient Hydrogen Evolution Photocatalyst *J. Am. Chem. Soc*. **136** 9280-3

[48] Chen H J, Yang Y L, Hong M, Chen J G, Suo G Q, Hou X J, Feng L and Chen Z G 2019 Separable and recyclable meso-carbon@TiO_2/carbon fiber composites for visible-light photocatalysis and photoelectrocatalysis *SM&T*. **21** e00105